Received: 30 November 2019 | Revised: 7 February 2020 | Accepted: 18 February 2020

DOI: 10.1002/ppap.201900243

FULL PAPER

PLASMA PROCESSES AND POLYMERS

Dissociation of tetramethylsilane for the growth of SiC nanocrystals by atmospheric pressure microplasma

Atta Ul Haq[1] | **Philip Lucke**[2] | **Jan Benedikt**[3] | **Paul Maguire**[1] | **Davide Mariotti**[1]

[1]Nanotechnology and Integrated Bioengineering Centre (NIBEC), Ulster University, Newtownabbey, UK

[2]Research Department of Plasmas with Complex Interactions, Ruhr-Universität Bochum, Bochum, Germany

[3]Institute of Experimental and Applied Physics, Faculty of Mathematics and Natural Sciences, Kiel University, Kiel, Germany

Correspondence
Atta Ul Haq and Davide Mariotti, Nanotechnology and Integrated Bioengineering Centre (NIBEC), Ulster University, Shore Road, Newtownabbey BT37 0QB, UK.
Email: au.haq@ulster.ac.uk (A. U. H.) and d.mariotti@ulster.ac.uk (D. M.)

Jan Benedikt, Experimental and Applied Physics, Faculty of Mathematics and Natural Sciences, Kiel University, 24098 Kiel, Germany.
Email: benedikt@physik.uni-kiel.de

Funding information
Engineering and Physical Sciences Research Council, Grant/Award Number: EP/R023638/1; Marie Curie Initial Training Network (RAPID), Grant/Award Number: 606889

Abstract

We report on mass spectrometry of residual gases after dissociation of tetramethylsilane (TMS) during the synthesis of silicon carbide (SiC) nanocrystals (NCs) by an atmospheric pressure microplasma. We use these results to provide details that can contribute to the understanding of the formation mechanisms of NCs. Mass spectrometry reveals the presence of high-mass polymerization products supporting the key role of neutral fragments and limited atomization. On this basis, we found that the loss of methyl groups from TMS, together with hydrogen abstraction, represents important paths leading to nucleation and growth. The combination of TMS concentration and NC residence time controls the NC mean size and the corresponding distributions. For higher precursor concentrations, the reaction kinetics is sufficiently fast to promote coalescence.

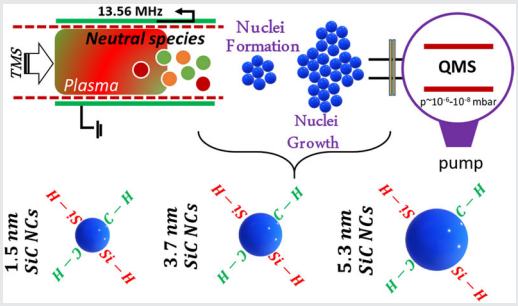

KEYWORDS
atmospheric pressure plasma, mass spectrometry, nanocrystals, silicon carbide, tetramethylsilane

1 | INTRODUCTION

Atmospheric pressure microplasma has shown impressive capabilities of synthesizing important nanoparticles and nanocrystals (NCs) with unique features and properties.[1–3] Microplasmas key features allow for the synthesis of ultrasmall nanoparticles and quantum dots with compositions that are most often complementary to low-pressure plasma processes. However, while low-pressure plasmas have been subject of extensive studies,[3–11] little is known about the formation mechanisms of nanoparticles in atmospheric pressure plasmas and diagnostic experimental results are limited.[1,12,13] In this contribution, we

have studied the concentration of species at the exit of a microplasma by mass spectrometry of residual gases. We have applied this diagnostic method to an atmospheric pressure argon microplasma mixed with tetramethylsilane (TMS) that has been previously used to synthesize ultrasmall silicon carbide (SiC) NCs.[14] The intent of this study is to produce relevant experimental results that could contribute to the understanding of the processes taking place within the microplasma and eventually support a description of the NC nucleation and growth mechanisms.

Organosilicon compounds, which contain C–Si bonds, have great significance in the scientific community as they have been used for the synthesis of various materials like SiC, SiN and SiC_xN_y.[15,16] TMS is a relatively simple organosilane, widely utilized as a precursor for the synthesis of many of these important materials[15–18] and is the simplest precursor used in the synthesis of SiC nanoparticles[19] and NCs.[14] SiC/SiC_xN_y films can potentially be significant for applications demanding thermal and mechanical stability.[20–25] These films can also be useful as low-cost wear/corrosion resistive coatings compared with diamond.[20] Furthermore, SiC NCs have shown beneficial properties for biological/optoelectronic applications[26] and catalytic applications, including water splitting and water purification.[27]

In this context, while the work is specifically carried out with Ar–TMS microplasmas, these results have general validity for a range of similar processes, precursors and NCs. Indeed, the fragmentation of TMS is also of wider interest to film deposition and other potential applications of these types of atmospheric pressure-operated microplasmas.

2 | EXPERIMENTAL DETAILS AND PRELIMINARY RESULTS

2.1 | Atmospheric pressure plasma setup and SiC NCs synthesis

The synthesis of SiC NCs was carried out in an atmospheric pressure microplasma reactor as previously reported[14]; this consists of a quartz glass tube of rectangular cross-section with two flat electrodes (20 × 5 mm), supplied with radiofrequency (RF) power (100 W) at 13.56 MHz. The plasma reactor was housed within an experimental setup (Figure 1) consisting of an RF power supply, gas chamber, plasma reactor, gas supplies, bubbler for storing TMS (Sigma-Aldrich), mass flow controllers, exhaust section and a stage for collecting the samples. The TMS bubbler was kept at room temperature (~18°C) with argon gas bubbled through at flow rates of 0.4, 2.4 and 5 sccm, while the total Ar gas flow was maintained constant at 1,000 sccm Ar. The deposition time of SiC NCs was 5–10 min and NCs were collected directly in ethanol keeping a gap of around 25 mm from the bottom of the capillary to the top of the vial.

Figure 2 shows the SiC NCs produced with this system where the gas flow rate through the TMS bubbler has determined the size and size distribution of the NCs. Full materials' characterization and the analysis of the optical properties were previously reported.[14]

2.2 | Quadrupole mass spectrometry and residual gas analysis (RGA)

The experimental setup for the RGA using a quadrupole mass spectrometer (QMS) is shown in Figure 3. RGA

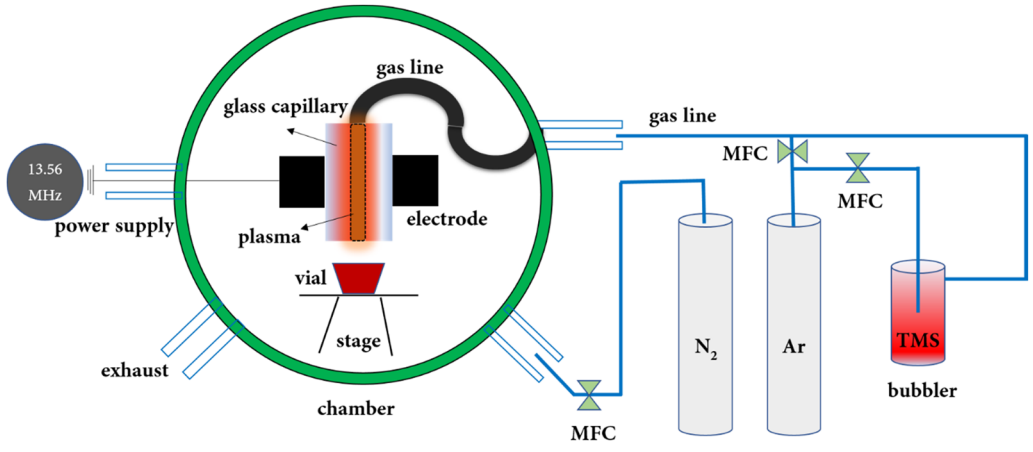

FIGURE 1 A schematic diagram of the experimental setup used to synthesize SiC nanocrystals in the atmospheric pressure plasma. Tetramethylsilane (TMS) is used as the precursor transported to plasma by Ar carrier gas. Mass flow controllers (MFCs) are used to control the gas flow rates

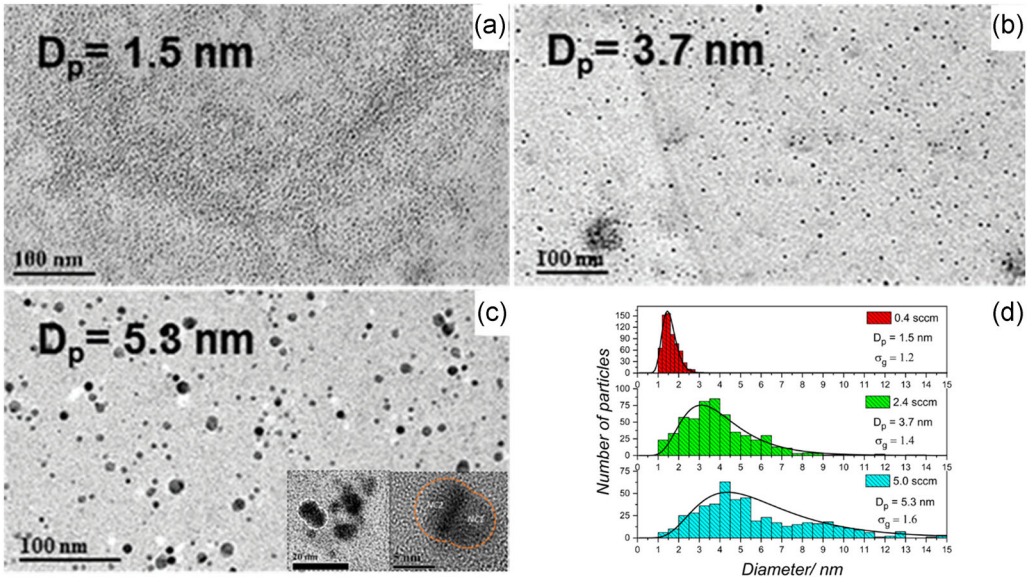

FIGURE 2 Low magnification transmission electron microscopy analysis for SiC nanocrystals produced at three different precursor flow conditions: (a) 0.4 sccm, (b) 2.4 sccm and (c) 5 sccm. The evidence of coalescing of nanocrystals at 5 sccm conditions are also shown as an inset in (c). (d) Corresponding size distribution determined from transmission electron microscopy images of SiC nanocrystals. The geometric mean value (D_p) and geometric standard deviation (σ_g) determined by fitting the experimental distribution with a log-normal distribution are also provided. Adapted with permission from Askari et al.[14]

measurements were carried out in a different experimental setup from the one used for the collection and characterization of the SiC NCs. This was due to the necessity of coupling the output of the microplasma to the QMS, which prevents a reliable and simultaneous collection of the SiC NCs. However, the setup for RGA measurements consisted of an exact replica of the microplasma reactor, gas and precursor supply and so on.

The residual gases, consisting of neutral species from the plasma, are filtered and the flow is controlled through an MFC (1–10 sccm). The residual gas is passed to a chamber where the pressure is maintained at 10 Pa. In the RGA setup, an electron impact ionizer with an electron energy of around 70 eV ionizes the neutral species in the gas. The generated ions are then passed to the quadrupole mass filter for their separation based on their mass to charge ratio (m/z). The mass-selected ion detection is performed with the help of the secondary electron multiplier. We should finally note that these RGA measurements rely on a very long transport path and, therefore, capture "well-mixed" densities of stable plasma chemistry products and the precursor molecules in the exhaust gas of the plasma source.

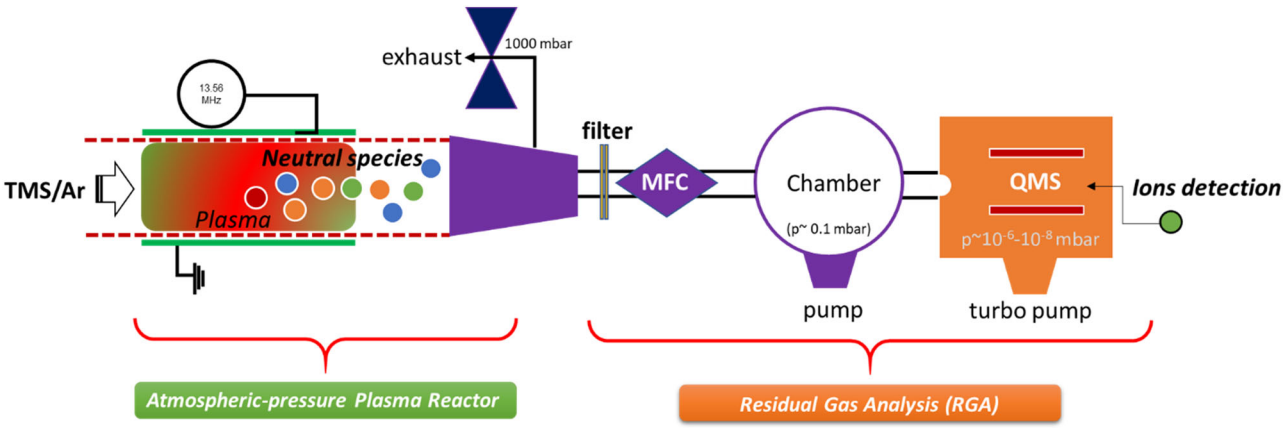

FIGURE 3 A schematic diagram showing the principles of the RGA using QMS. The residual gases produced in our plasma synthesis of SiC nanocrystals using the plasma configurations as shown in the figure. The tetramethylsilane gas is carried to the plasma reactor using the argon gas through the bubbler. MFC, Mass flow controller; QMS, quadrupole mass spectroscopy

2.3 | Introduction to TMS mass spectrometry measurements

TMS (Si–$(CH_3)_4$) has been extensively used as a precursor for the growth of SiC or Si products.[28,29] TMS usually dissociates into fragments by the loss of the methyl group(s) (CH_3) where the C–Si bonds are broken.[30] As a result, the most common fragment by far is trimethylsilyl ($Si(CH_3)_3$) with other common fragments being methyl (CH_3), dimethylsilyl ($Si(CH_3)_2$), dihydromethylsilyl (H_2SiCH_3) and silicon (Si). In the RGA, TMS and many other organosilicon compounds do not form stable molecular ions under electron impact ionization as they are prone to lose one methyl group and are, therefore, detected at mass 15 amu smaller than their molecular mass (e.g., the TMS is detected at m/z of 73 amu and not 88 amu). Additionally, the high electron energy of 70 eV also leads to further fragmentation of ionized molecules and a so-called fragmentation or cracking pattern is generated for any molecular species.[31,32] One m/z ratio may contain signals from multiple fragment ions generated within the RGA by dissociative ionization. Any signal at a given m/z must, therefore, be checked for possible contributions from different parent molecules.

The RGA analysis was performed with three gas flow conditions, that is, 0.4, 2.4 and 5 sccm and at an RF applied power of 120, 150 and 190 W, respectively. The total argon gas flow was constant at 1,000 sccm. Argon gas was also bubbled through the TMS bubbler at flow rates of 0.4, 2.4 and 5 sccm.

The relative changes in the signal are detected at plasma "ON" and "OFF" conditions. During plasma OFF, the reference level is measured so that relative changes at plasma ON can be evaluated. The signal is normalized to argon signal (40 amu) to eliminate any drift of the mass spectrometer signal over time. This normalized signal can also be used as a rough estimation of the species concentrations because the gas mixture at one atmosphere is dominated by Ar gas. To obtain a more accurate concentration estimation, the argon ionization cross-section and the ionization cross-section at the electron energy of 70 eV should be taken into consideration. However, this absolute calibration is not performed here because ionization cross-sections are not known for most of the measured species. Therefore, the signal at 73 amu (= 88–15 amu) is instead taken as a reference for the amount of TMS in the gas (during OFF conditions) and in the plasma (during ON conditions) and is expected to decrease with increasing fragmentation. Plasma OFF/ON and other TMS concentration/power conditions have been applied consecutively and alternatively (see Figure 4), that is, from 0 to 40 min at 5 sccm, from 40 to

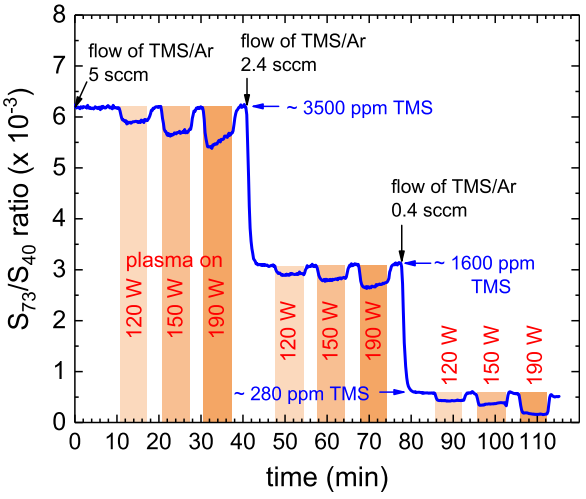

FIGURE 4 The change of the tetramethylsilane (TMS) signal at $m/z = 73$ (normalized to the Ar reference signal at mass 40) during the experiment with three different TMS admixtures and applying three different powers

78 min at 2.4 sccm and from 78 min at 0.4 sccm. At each of the three flow settings, the plasma was in the ON state three times for 400 s at each of the three applied RF powers (120, 150 and 190 W). The interval between plasma ON conditions was selected such that the TMS signal increased to the level before switching on the plasma. The plasma ON regions in Figure 4 clearly confirm the consumption of TMS due to plasma-driven dissociation and polymerization reactions at different powers and TMS/Ar gas flow rates.

The concentration of TMS in the plasma at 5, 2.4 and 0.5 sccm is estimated using the following relation:

$$\text{Flow of TMS} = F \times \text{flow of Ar (bubbler)}, \tag{1}$$

where F stands for the temperature-dependent scaling factor for TMS flow in the Argon flow through the bubbler.

$$F(T) = \frac{p_{\text{vapour,TMS}}(T)}{1\,\text{atm} - p_{\text{vapour,TMS}}(T)}, \tag{2}$$

where $p_{\text{vapour,TMS}}(T)$ represents the TMS vapour pressure at a given temperature. F was found to be around 0.7 (with $p_{\text{vapour,TMS}}(T) = 0.41$ atm at $T = 3$°C of the TMS in the bubbler) giving TMS concentrations of around 3,500 ppm (0.35%), 1,600 ppm (0.16%) and 280 ppm corresponding to the three Ar bubbler flow conditions.

The TMS concentration is not always constant during the plasma ON period, in particular, at the highest applied powers, where it decreases sharply shortly after the plasma is ignited but then increases over time while the

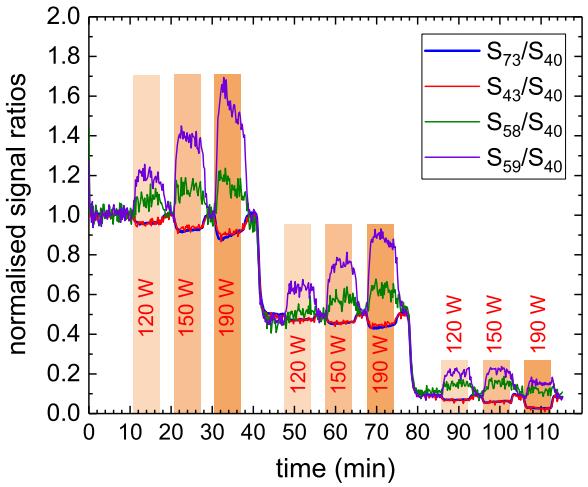

FIGURE 5 The change of the signal ratios normalized to their values at plasma OFF (time range from 0 to 10 min) to demonstrate the baseline correction by the masses with contribution from fragment ions of the tetramethylsilane

plasma is still ON; see, for example, the signal change between 30 and 38 min in Figure 4. The same temporal evolution is also observed in the measurements of other plasma chemistry products (Figure 5) and it is a likely consequence of the increasing temperature in the plasma reactor (including cables, matching unit components etc.) and/or changing wall conditions in the capillary (e.g., deposition). This effect is further amplified with a progressive deviation from ideal electrical matching conditions, which is more obvious at high power (e.g., 190 W). Therefore, to ensure consistency of our analysis, we will consider measurements corresponding to values taken shortly after turning the plasma on.

3 | RESULTS AND DISCUSSION

3.1 | Preliminary results and assumptions

The signals at $m/z = 2$, 15, 16, 26, 27, 28, 30, 32, 40, 43, 45, 58, 59, 117, 129, 131 and 145 have been measured together with the TMS at $m/z = 73$ (see Table 1); no other signals were detected within the available range (up to $m/z = 200$). The m/z signals that scales with the TMS signal under plasma OFF conditions are very likely ions generated by the RGA dissociative electron impact ionization.

Assuming in the first approximation that the signal measured at $m/z = 73$ amu is only due to TMS fragmentation and ionization within the RGA (without contribution due to plasma dissociative ionization of some heavier polymerization products formed in the plasma

TABLE 1 m/z signals monitored in our experiments with ions and our assignments are reported

m/z (amu)	Ion	Assigned parent species
2	H_2^+	H_2
15	CH_3^+	CH_3, CH_4, methylsilanes
16	$^{**}CH_4^+$	$^{*}CH_4$
26	$C_2H_2^+$	mainly C_2H_2
27–30	$C_2H_x^+$	C_2H_4, C_2H_6
40	Ar^+	Ar
43	$SiCH_3^+$	TMS
58	$Si(CH_3)_2^+$	$^{***}Si(CH_3)_3$
59	$HSi(CH_3)_2^+$	$^{***}HSi(CH_3)_3$
73	$Si(CH_3)_3^+$	TMS
117	$(CH_3)_3Si–Si(CH_3)H^+$	$(CH_3)_3Si–Si(CH_3)_2H$
129	$(CH_3)_2Si(CH_2)_2Si(CH_3)^+$	$(CH_3)_2Si(CH_2)_2Si(CH_3)_2$
131	$(CH_3)_3Si–Si(CH_3)_2^+$	$(CH_3)_3Si–Si(CH_3)_3$
145	$(CH_3)_3Si(CH_2)Si(CH_3)_2^+$	$(CH_3)_3Si(CH_2)Si(CH_3)_3$

Note: Some of the measured signals have been corrected by subtracting (*) H_2O, O_2, (**) O^+ and (***) TMS.
Abbreviation: TMS, tetramethylsilane.

chemistry), all signals can be normalized with respect to 73 amu at the highest flow. Once normalized, the results clearly show (Figure 5) that $m/z = 43$ are only fragment ions of TMS because they behave in the same way as the signal at m/z of 73 amu; these fragment ions are, in fact, reported in the TMS fragmentation pattern reported in the literature.[33] This corroborates also our assumption that $m/z = 73$ is representative for TMS. The ions detected at m/z of 58 and 59 amu are fragment ions of the TMS as well because they are detected under plasma OFF conditions. However, the signal under plasma on conditions does not follow the measured signal at m/z of 73 or 43 amu, which indicates that species generated in the plasma are also contributing to these signals. To obtain proper signal change for the $m/z = 58$ and 59 amu upon plasma ignition, the changing background signal due to the TMS fragment ions has to be subtracted from the measured signal, for example, by subtracting the normalized S_{73}/S_{40} signal ratio from the normalized S_{59}/S_{40} signal ratio.

Some measured signals have constant background signal for all set TMS concentrations. This background signal is due to background species in the QMS (e.g.,

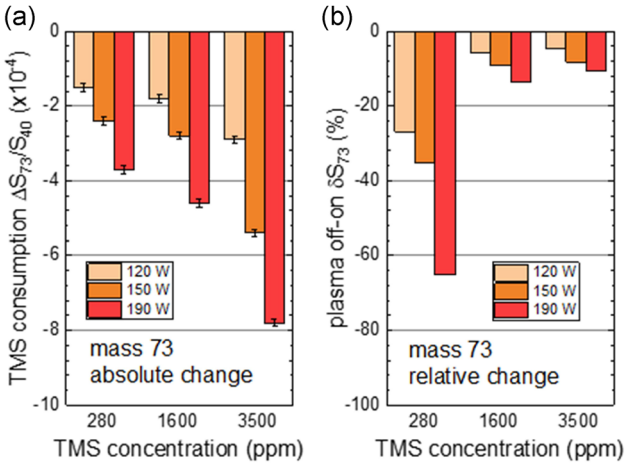

FIGURE 6 Tetramethylsilane (TMS) (a) absolute consumption and (b) relative to the OFF signal

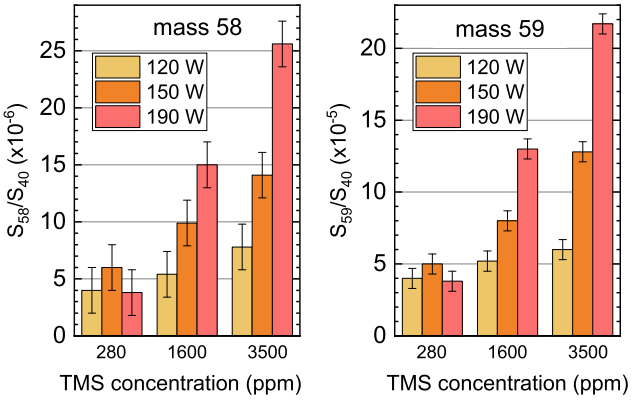

FIGURE 7 Signals at $m/z = 58$ and 59 corrected for the background signal (see Figure 5 and corresponding text for details) originating very probably from dissociative ionization of trimethylsilane. Note that the *y* axis of the two figures report values with one order of magnitude difference

O^+ signal at $m/z = 16$ amu due to RGA dissociative ionization of H_2O or O_2 background molecules) and it is therefore present under plasma ON conditions as well. This constant background can be, therefore, easily subtracted from the measurements at, for example, m/z of 16 amu. Finally, it should be noted that the larger polymerization products have no background signal and are detected only during the plasma ON time.

3.2 | Measurement of species

TMS absolute consumption is determined from $\Delta S_{73}/S_{40} = (S_{73\text{-ON}} - S_{73\text{-OFF}})/S_{40\text{-OFF}}$ and shows (Figure 6a) that TMS consumption increases with power and TMS flow rate, as expected since the higher power levels lead to increased dissociation while higher TMS flow, and hence concentration, accelerates polymerization reactions. The relative percent consumption (Figure 6b), however, from $\delta S_{73} = (S_{73\text{-ON}} - S_{73\text{-OFF}})/S_{73\text{-OFF}}$, is greatest under the lowest TMS flow conditions, reaching 65% at 190 W applied power. This is due to the increased energy per TMS molecule available at lower TMS concentrations and higher power.

Figure 6b also shows that full dissociation of TMS is not reached as it is likely that the power applied per TMS molecule can be rather low considering the strongly collisional regime where energy goes into a range of mechanisms including ionization, rotational and vibrational excitation as well as heating; we should also note that while the applied power is high, the matching conditions ultimately allow for delivering <10 W to the plasma. Due to the consumption of TMS, other species are formed and detected at other m/z values. The most probable dissociation path of TMS in plasma is a loss of one or several methyl groups. The signals at $m/z = 58$ and 59 amu exhibit similar characteristics to S_{73} with plasma conditions (Figure 5); their relative ratio in Figure 7 corresponds to the fragment ratio from the fragmentation pattern of the trimethylsilane $HSi(CH_3)_3$. Ions originating from molecules with fewer methyl groups have not been detected and therefore trimethylsilane appears to be the main TMS fragmentation product due to dissociation in the plasma, indicating the possible contribution of these molecules to NCs synthesis. At the lowest TMS flow and concentration (Figure 7), the signal shows little, if any, dependence on power and this may be due to the participation of trimethylsilane in other plasma-induced reactions and or contributing to the synthesis of NCs.

The TMS fragments can further react with TMS and other formed molecules and lead to larger polymerization products. Figure 8 shows the signals detected at masses larger than $m/z = 73$ amu, that is, at $m/z = 117$, 129, 131 and 145 amu. Comparing the fragmentation patterns from NIST Chemistry Webbook,[33] the species that could be responsible for these signals can be assigned (see Table 1). Again, the parent molecules have $m/z = 15$ amu higher (all these molecules lose a methyl group after dissociation). The signal at $m/z = 117$ amu is the weakest and noisiest of all polymerization products. The signal at $m/z = 131$ amu, also weak and noisy, could correspond to hexamethyldisilane $Si_2(CH_3)_6$ from the reaction of two Si $(CH_3)_3$ radicals or $Si(CH_3)_3$ radical with TMS. The signal at $m/z = 145$ amu, very probably methylenebis(trimethylsilane), is the most logical first step polymerization product as it also has the highest signal with lowest noise and is dominant at very high TMS concentrations. This could originate from the reaction of $Si(CH_3)_3$ radicals with TMS. The involvement of trimethylsilane ($m/z = 58$ and 59; Figure 7) in the production of these larger polymerization

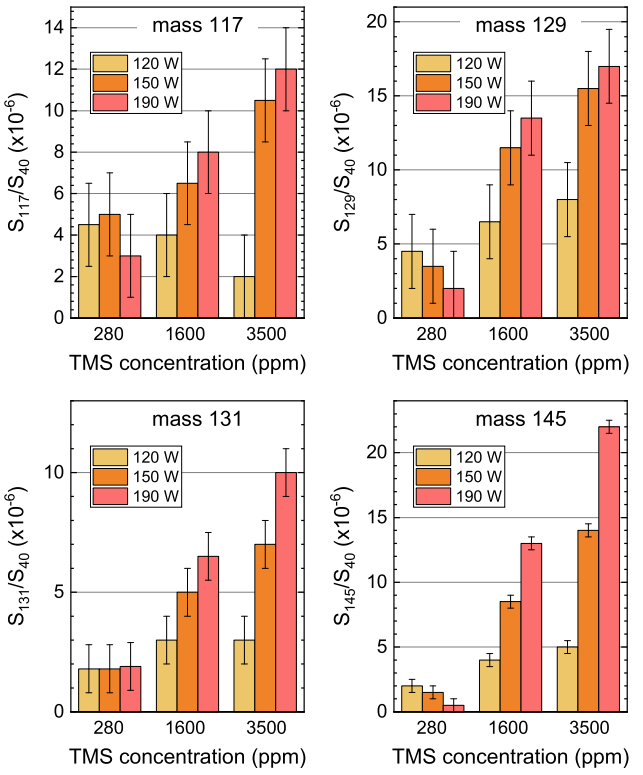

FIGURE 8 Signals of larger organosilicon molecules. TMS, tetramethylsilane

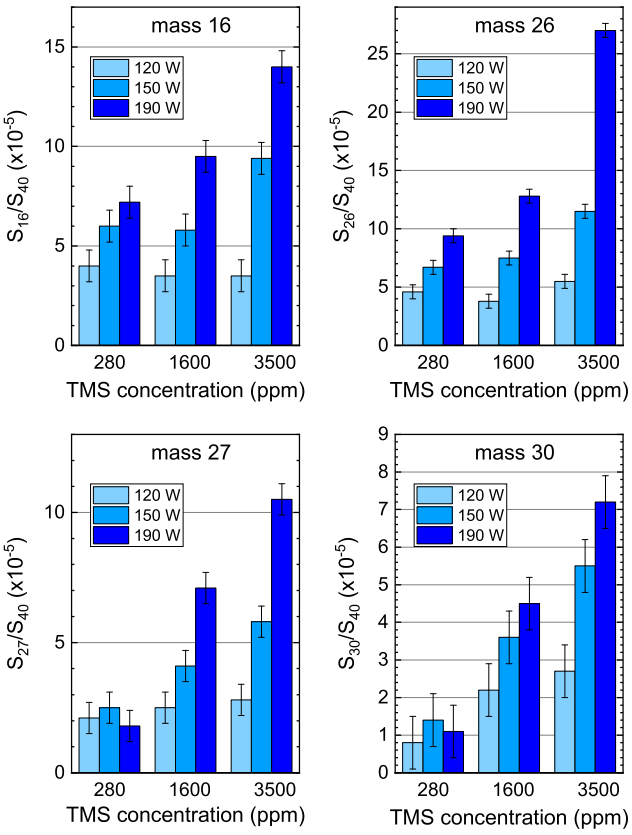

FIGURE 9 Signals of hydrocarbon molecules. TMS, tetramethylsilane

products is confirmed by the similar trends at the lowest concentrations (280 ppm). We have observed that at the lowest TMS concentration (280 ppm), increasing the power can reduce the presence of these larger mass molecules indicating a relatively low stability within the plasma environment and that they are prone to further fragmentation. The products at $m/z = 117$ and 131 amu appear to be less sensitive to power (280 ppm in Figure 8), which suggest that Si–Si bonds are more resilient than the C–C bonds in these molecular configurations; the former have, in fact, been found to contribute to deposition in low-pressure plasma processes.[34]

Additionally, H_2, CH_4 and other hydrocarbons are generated from methyl groups (Figures 9 and 10). At $m/z = 16$ amu, the signal may also correspond to methanol (CH_3OH) formed from the methyl groups, from TMS fragmentation, an expected side product, next to H_2, of the TMS plasma chemistry.[31,35] The signal at $m/z = 26$ amu is the parent ion of C_2H_2, which is the most stable C_2H_x hydrocarbon under plasma conditions[35,36] and result in the highest signal compared with $m/z = 27$ and 30 amu. Signals at $m/z = 27$ and 30 amu are, therefore, fragment ions from C_2H_x molecules. C_2H_2 can be formed from the dissociation of C_2H_4 or C_2H_6 which is corroborated by the increasing m/z signal at 26 amu with increasing power with 280 ppm TMS, where the 27 and 30 amu signals are decreasing. H_2 signal at $m/z = 2$ amu is largest under low TMS admixture and highest power, which is a strong indication for effective dissociation and high reactivity of the plasma under these conditions.

These results suggest that when the TMS concentration is sufficiently high, plasma dissociation contributes to supply fragments for subsequent polymerization. This is supported by our results at 1,600 and 3,500 ppm where

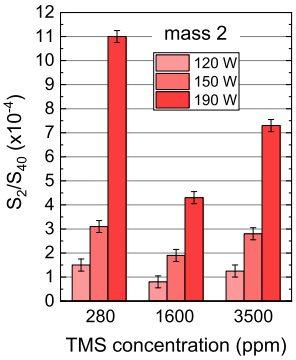

FIGURE 10 Signal at $m/z = 2$ corresponding to molecular hydrogen. TMS, tetramethylsilane

we see the largest products to increase with power. However, when the TMS concentration is low and plasma power is high, dissociation can dominate. This is corroborated by a large increase in molecular hydrogen (Figure 10) at 280 ppm where its concentration is the highest even compared to conditions with much higher TMS concentrations in the gas mixture.

3.3 | Discussion of the plasma chemistry pathways

Fragmentation of TMS initially results in the loss of CH_3 groups (CH_3 signal with $m/z = 15$ due to CH_3 radical and CH_4 molecule) which can be also seen in the formation of $Si(CH_3)_3$ ($m/z = 58$) and $HSi(CH_3)_3$ ($m/z = 59$), where in the latter an H atom has terminated the Si bond. Furthermore, lighter species such as H_2, CH_4 (and possibly relatively unreactive CH_3 as well) and hydrocarbons with two carbon atoms are generated from these fragments. The follow-up reactions are then strongly dependent on the TMS concentration and can be divided into two cases.

At the lowest TMS concentration of 280 ppm, the TMS depletion reaches 73% at the largest applied power. The low probability of polymerization reaction is due to the low TMS concentration as polymerization products presented in Figure 8 have very low signals and they are even decreasing with increasing power. The fragment concentrations are constant or decreasing with increasing power indicating that they are, after being generated, further dissociated into even smaller fragments. This is corroborated by the steep increase of H_2 signal intensity and increasing signals of CH_4 and C_2H_2, the most stable hydrocarbons under plasma conditions.

When the TMS concentration is higher (1,600 ppm or higher), the absolute TMS consumption increases, but the relative depletion stays below 15% because much more TMS is available in the plasma. Both the signal intensity of TMS fragments (Figure 7) and polymerization products (Figure 8) are increasing both with increasing TMS concentration and increasing applied power. Therefore, the main follow-up reactions of primary TMS fragments appears to be polymerization reactions leading to the formation of larger molecules. However, increasing the concentration of the TMS from 1,600 to 3,500 ppm does not result in the proportional increase (expected to be by a factor of 2.2 based on the ppm ratio) of the signal intensities indicating that both the formation of fragments and the resulting polymerization is limited by the ability of the plasma to couple sufficient power to promote the initial fragmentation.

3.4 | NCs formation mechanisms

A direct and accurate relationship between the SiC NCs synthesis conditions and the plasma conditions during the RGA measurements is complicated by many factors including power delivered, matching conditions and bubbler temperature, also in consideration that the two set of experiments (i.e., NC synthesis and RGA measurements) were carried out separately and necessarily in different experimental setups, even when identical microplasma reactor replicas are used. Our experimental work (leading to our published reports[14,37]) has demonstrated NC synthesis for a very broad range of plasma conditions; within this broad parameter space, NCs size, size distribution, surface states and possibly defect densities have mainly varied. We can, however, estimate that the conditions used for the synthesis of 1.5 nm NCs are closest to the RGA measurements produced at 1,600 ppm at 120 W. Consequently, the larger SiC NCs (mean diameter of 3.7 and 5.3 nm) can be qualitatively represented by the RGA measurements obtained at 120 W and TMS concentrations larger than 1,600 ppm, that is, 3,500 ppm. Therefore, the conditions replicated during our RGA measurements are, of course, expected to lead to NC nucleation and growth, however, we believe that the analysis of the NC formation mechanisms must remain mostly qualitative due to some degree of deviation in the properties characterizing the SiC NCs.

This atmospheric pressure microplasma is characterized by typical electron densities and gas temperatures in the ranges of ~10^{14} cm^{-3} and 410–490 K, respectively. These were measured by emission spectroscopy analyzing the atomic H line and OH lines. We also observed that the inclusion of various precursors, while perturbing the plasma at some extent, did not drastically change the values of these parameters' ranges. At these conditions we have evaluated, through a theoretical model, that the electron temperature is about ~1 eV and nanoparticles within the plasma can reach temperatures close to 1,000 K due selective heating. The crystallization temperature of SiC is expected to be much lower than the bulk value (~1,473 K)[38] and therefore particles growing within the plasma would experience temperatures sufficiently high to promote crystallization.

We do not expect the nucleation phase to be determined by full atomization of silicon and carbon atoms that subsequently aggregate due to high number densities. The reason for this is that stoichiometric SiC has been produced under a range of different conditions, including this study and others,[37] which require a 1:1 ratio of Si and C atoms being present in the gas phase. As we observed, in our transmission electron microscopy (TEM) analysis, neither mixed phase NCs nor

NCs formed from elemental Si or C, we believe it unlikely that this ratio can be maintained in all synthesis conditions and hence NC nucleation is largely determined by initial polymerization reactions among TMS fragments.

While in a low-pressure plasma, anions can play a very important role in the polymerization chain reactions,[3] these can be excluded from any critical role here due to the much lower ionization degree found in atmospheric pressure plasmas.[5,39] Furthermore, the confinement of anions in the bulk of low-pressure plasmas is generally not observed at atmospheric pressure due to an expanding sheath and the oscillating nature of the bulk plasma which is also characterized by the presence of strong electric fields.[40] We, therefore, conclude that nucleation is essentially determined by initial polymerization reactions of neutral species; interactions among neutral species/radicals are enhanced by the atmospheric pressure regime which increases the collision frequency among neutrals being present at much higher densities.

The initial reactions are very likely the result of TMS molecules and $H_xSi(CH_y)_z$ fragments (including $m/z = 58$ and 59) reacting among themselves and aided by either the loss of methyl groups, the loss of hydrogen atoms or by H-abstraction such as:[34]

$$(CH_3)_3Si + CH_2(CH_3)_3Si \rightarrow (CH_3)_3Si{-}CH_2(CH_3)_3Si, \quad (3)$$

$$Si(CH_3)_3H_3C + HSi(CH_3)_3 \rightarrow Si(CH_3)_3H_2C{-}Si(CH_3)_3 + H_2. \quad (4)$$

The formation of molecular hydrogen resulting from H-abstraction is confirmed by our RGA results in Figure 10. While we observe higher molecular weight polymerization products (Figure 8), products resulting from reactions (3) and (4) are not observed, supporting the argument that these reactions represent pathways to NC formation and therefore the products are scavenged from the microplasma before reaching the RGA. We also observe that the polymerization products at $m/z = 117$ and 131 (Figure 8) require the same precursor fragments as for the NC growth above, while $m/z = 129$ and 145 rely on different fragments for their formation. Looking at the data obtained at 120 W, the latter ($m/z = 129$ and 145; Figure 8) increase with TMS concentration, while the former ($m/z = 117$ and 131; Figure 8) are reduced when TMS is increased ($m/z = 117$ in particular), therefore supporting the hypothesis of lower mass fragments consumption in NC growth. On this basis, it is reasonable to say that the loss of a higher number of methyl groups from TMS favours NC growth.

Following initial nucleation, these reactions can also explain the growth of the NCs as the growing chain will result in branching thereby creating a three-dimensional network. The formation of the SiC NCs necessarily requires the formation of "transverse" bonds between Si and C atoms present in the polymerized networks, which can also occur through the reactions (3) and (4) outlined above or simply by cross-linking two neighbouring dangling bonds of Si– and C–.

The nucleation and growth phases described above are supported by our comments on atomization, anions and by our QMS results. Furthermore, this type of growth is fully consistent with the surface properties of the NCs which exhibit H-terminations at the surface C-sites as it would result from the polymerization process. In contrast, based on the reactions above, Si atoms would either be bonded to C atoms or remain exposed to the environment and therefore prone to develop hydrogen terminations within the plasma or lead to immediate oxidation when exposed to the atmosphere. In fact, our surface analysis has revealed H-terminations on carbon/silicon atoms and selective oxidation at the Si sites,[14] therefore corroborating the nucleation and growth processes suggested here.

Finally, the synthesis experiments clearly show that by increasing the TMS concentration, larger NCs are produced, which are likely to result from the fast reactions of generated fragments with abundant TMS molecules, accelerating the polymerization reactions and increasing the size and number of NCs produced per time. In these cases, as neither the fragments nor the higher mass products are depleted, the growth and resulting size are, therefore, determined by the residence time (constant in the two cases) and by the initial TMS concentration, but in general, it is neither reaction-limited, diffusion-limited, nor limited by the supply of precursors. This is corroborated by the results of Figure 7 ($m/z = 58$, 59), which show that the fragments participating in the polymerization reactions increase with increasing TMS concentration. However, at the highest TMS concentration leading to NC with 5.3 nm diameter, the TEM analysis reveals evidence of coalescence with some particles having nonspherical shapes (Figure 2c) and an increase in mean size largely due to a broadening of the distribution and the appearance of a bimodal distribution peaking just above ~4 and ~9 nm (Figure 2d). At the highest concentration, the reaction kinetics may be sufficiently fast to produce a high spatial density of NCs, which through multiple neighbouring collisions lead to coalescence. Evidence of coalescence as per insets of Figure 2c, was not found for the synthesis conditions of the smaller NCs; however, we can acknowledge that the size distribution of the NCs with 3.7 nm mean diameter

may exhibit the initial development of a bimodal distribution with a second peak possibly appearing above 6 nm. The size distribution of the smallest NCs is much narrower and therefore we do not expect coalescence to play a major role in this case.

4 | CONCLUSION

Dissociation of TMS in the plasma at atmospheric pressures was investigated by analysing the residual gases formed in the plasma with the help of QMS. This study revealed the dissociation and polymerization of the TMS in the plasma, which are dependent on the concentrations of TMS and applied power. It was found that the consumption of TMS is more effective at low TMS concentrations (280 ppm) compared with their consumptions at high concentrations (3,500 ppm) due to higher available power per TMS molecule. The highest measured TMS depletion was only 73% (280 ppm) and therefore full atomization of TMS molecules was not achieved, excluding the possibility of NC nucleation initiated by aggregation of Si and C atoms. The lower relative TMS depletion (<15%), but larger absolute TMS consumption and formation of larger polymerization products are observed under conditions with higher TMS concentrations. These observations and our assumptions suggest that the formation mechanism of SiC NCs in the Ar/TMS atmospheric plasma is the polymerization reactions of neutral TMS fragments where the resident time and TMS concentration play the main role in determining the size and the size distribution of the NPs. The main difference from low-pressure plasma is the importance of neutral species and the limited contribution of ions.

ACKNOWLEDGMENTS

The authors acknowledge the support from the Marie Curie Initial Training Network (RAPID-ITN, Award No. 606889) and from the Engineering and Physical Sciences Research Council (EPSRC, Award No. EP/R023638/1).

ORCID

Atta Ul Haq http://orcid.org/0000-0002-3942-6290
Jan Benedikt http://orcid.org/0000-0002-8954-1908
Paul Maguire http://orcid.org/0000-0002-2725-4647
Davide Mariotti http://orcid.org/0000-0003-1504-4383

REFERENCES

[1] S. Askari, M. Macias-Montero, T. Velusamy, P. Maguire, V. Svrcek, D. Mariotti, *J. Phys. D: Appl. Phys.* **2015**, *48*, 314002.
[2] D. Mariotti, T. Belmonte, J. Benedikt, T. Velusamy, G. Jain, V. Švrček, *Plasma. Process. Polym.* **2016**, *13*, 70.
[3] U. R. Kortshagen, R. M. Sankaran, R. N. Pereira, S. L. Girshick, J. J. Wu, E. S. Aydil, *Chem. Rev.* **2016**, *116*, 11061.
[4] A. Garscadden, *Pure Appl. Chem.* **1994**, *66*, 1319.
[5] U. Kortshagen, *J. Phys. D: Appl. Phys.* **2009**, *42*, 113001.
[6] N. Rao, S. Girshick, J. Heberlein, P. McMurry, S. Jones, D. Hansen, B. Micheel, *Plasma Chem. Plasma Process.* **1995**, *15*, 581.
[7] D. Coleman, T. Lopez, O. Yasar-Inceoglu, L. Mangolini, *J. Appl. Phys.* **2015**, *117*, 193301.
[8] V. Vekselman, Y. Raitses, M. N. Shneider, *Phys. Rev. E* **2019**, *99*, 063205.
[9] M. Mao, J. Benedikt, A. Consoli, A. Bogaerts, *J. Phys. D: Appl. Phys.* **2008**, *41*, 225201.
[10] S. L. Girshick, C.-P. Chiu, *Plasma Chem. Plasma Process.* **1989**, *9*, 355.
[11] J. Perrin, C. Bohm, R. Etemadi, A. Lloret, *Plasma Sources Sci. Technol.* **1994**, *3*, 252.
[12] S. Askari, I. Levchenko, K. Ostrikov, P. Maguire, D. Mariotti, *Appl. Phys. Lett.* **2014**, *104*, 163103.
[13] N. J. Kramer, E. S. Aydil, U. R. Kortshagen, *J. Phys. D: Appl. Phys.* **2015**, *48*, 035205.
[14] S. Askari, A. Ul Haq, M. Macias-Montero, I. Levchenko, F. Yu, W. Zhou, K. (Ken) Ostrikov, P. Maguire, V. Svrcek, D. Mariotti, *Nanoscale* **2016**, *8*, 17141.
[15] S. Peter, R. Pintaske, G. Hecht, F. Richter, *Surf. Coat. Technol.* **1993**, *59*, 97.
[16] E. N. Ermakova, S. V. Sysoev, L. D. Nikulina, I. P. Tsyrendorzhieva, V. I. Rakhlin, M. L. Kosinova, *Thermochim. Acta.* **2015**, *622*, 2.
[17] N. Zaitseva, S. Hamel, Z. R. Dai, C. Saw, A. Williamson, G. Galli, *J. Phys. Chem. C* **2008**, *112*, 3585.
[18] A. Baby, C. M. O. Mahony, P. D. Maguire, *Plasma Sources Sci. Technol.* **2011**, *20*, 015003.
[19] H. Lin, J. A. Gerbec, M. Sushchikh, E. W. McFarland, *Nanotechnology* **2008**, *19*, 325601.
[20] N. I. Fainer, *Russ. J. Gen. Chem.* **2012**, *82*, 43.
[21] M. Bhatnagar, B. J. Baliga, *IEEE Trans. Electron Devices* **1993**, *40*, 645.
[22] H. Morkoç, S. Strite, G. B. Gao, M. E. Lin, B. Sverdlov, M. Burns, *J. Appl. Phys.* **1994**, *76*, 1363.
[23] C. I. Harris, S. Savage, A. Konstantinov, M. Bakowski, P. Ericsson, *Appl. Surf. Sci.* **2001**, *184*, 393.
[24] Y. Ben-Zion, *J. Geophys. Res.* **2002**, *107*, 2042.
[25] H. L. Chang, C. T. Kuo, *Mater. Chem. Phys.* **2001**, *72*, 236.
[26] J. Fan, H. Li, J. Jiang, L. K. Y. So, Y. W. Lam, P. K. Chu, *Small* **2008**, *4*, 1058.
[27] Y. Zhang, T. Xia, P. Wallenmeyer, C. X. Harris, A. A. Peterson, G. A. Corsiglia, J. Murowchick, X. Chen, *Energy Technol.* **2014**, *2*, 183.
[28] J. M. Lemieux, J. Zhang, *Int. J. Mass Spectrom.* **2014**, *373*, 50.
[29] X. M. Li, B. D. Eustergerling, Y. J. Shi, *Int. J. Mass Spectrom.* **2007**, *263*, 233.
[30] Mass Spectrum of Tetramethylsilane, https://webbook.nist.gov/cgi/cbook.cgi?Name=TMS&Units=SI&cMS=on (accessed: August **2017**).
[31] R. Basner, R. Foest, M. Schmidt, F. Sigeneger, P. Kurunczi, K. Becker, H. Deutsch, *Int. J. Mass Spectrom. Ion Processes* **1996**, *153*, 65.

[32] J. Benedikt, A. Hecimovic, D. Ellerweg, A. von Keudell, *J. Phys. D: Appl. Phys.* **2012**, *45*, 403001.
[33] P. Linstrom, NIST Mass Spectrometry Data Center, *NIST Chemistry WebBook, NIST Standard Reference Database Number 69* (Eds: P. J. Linstrom, W. G. Mallard), National Institute of Standards and Technology, Gaithersburg, MD **1997**.
[34] J. L. C. Fonseca, D. C. Apperley, J. P. S. Badyal, *Chem. Mater.* **1993**, *5*, 1676.
[35] A. Soum-Glaude, L. Thomas, A. Dollet, P. Ségur, M. C. Bordage, *Diamond Relat. Mater.* **2007**, *16*, 1259.
[36] J. Benedikt, *J. Phys. D: Appl. Phys.* **2010**, *43*, 043001.
[37] J. McKenna, J. Patel, S. Mitra, N. Soin, V. Švrček, P. Maguire, D. Mariotti, *Eur. Phys. J.: Appl. Phys.* **2011**, *56*, 24020.
[38] T. Rajagopalan, X. Wang, B. Lahlouh, C. Ramkumar, P. Dutta, S. Gangopadhyay, *J. Appl. Phys.* **2003**, *94*, 5252.
[39] A. Gallagher, A. A. Howling, C. Hollenstein, *J. Appl. Phys.* **2002**, *91*, 5571.
[40] A. J. Wagner, D. Mariotti, K. J. Yurchenko, T. K. Das, *Phys. Rev. E* **2009**, *80*, 065401.

How to cite this article: Ul Haq A, Lucke P, Benedikt J, Maguire P, Mariotti D. Dissociation of tetramethylsilane for the growth of SiC nanocrystals by atmospheric pressure microplasma. *Plasma Process Polym*. 2020;17:e1900243. https://doi.org/10.1002/ppap.201900243